

# RF PINGER COMMISSIONING AND BEAM DYNAMICS STUDIES AT NSLS-II\*

G-M. Wang<sup>†</sup>, Timur Shaftan, James Rose, Victor Smaluk, Yongjun Li, Brian Holub

Brookhaven National Laboratory, Upton, NY

## Abstract

Similar to the pinger commonly used for transverse beam dynamic studies, we developed and commissioning the RF pinger -- a short pulse kicker in the longitudinal plane. During recent beam studies we shifted the RF phase within a short interval of time (much less than the synchrotron period). Using turn-by-turn (TBT) BPM data we carried out several experiments, i.e. measured the NSLS-II ring momentum aperture with and without damping wigglers, located the momentum aperture limitation and initiated beam crossing major resonance under the stopband width control. This paper presents our initial beam study results.

## INTRODUCTION

“RF pinger”, defined as a sudden change to RF phase or voltage serves to induce longitudinal oscillation. This technique is known in accelerators and has been used in, for instance,  $\gamma_T$ -crossing in hadron machines [1], dispersion measurements at ATF and SLC [2], pulse length manipulation with RF phase jump [3]. Similar to the short-pulse transverse kick-pinger commonly used for transverse beam studies, RF jump presents a powerful tool for investigation of the beam dynamics.

NSLS-II storage ring low-level RF (LLRF) system has digital ramp control function, which enables rapid change of the cavity phase and amplitude. RF pinger is triggered on demand via timing system and is synchronized with other systems triggered via timing, such as BPMs or transverse pingers. LLRF controller has the fast digital acquisition function helpful for capturing the RF system data and relevant beam information. Using the RF phase jump, we measured machine momentum aperture with and without damping wigglers (DW), assessed aperture limit location along the ring and studied beam crossing half integer resonance while controlling the stopband width.

## NSLS II RF SYSTEM

NSLS-II is a 3 GeV storage ring synchrotron light source [4, 5]. The storage ring lattice is designed with 2 RF straight sections each having two 499.68 MHz superconducting (SRF) single cell cavities. The RF cavities were installed and commissioned to the RF voltage up to 1.8 MV.

SR RF system [6, 7] consists of digital LLRF controllers [8], 300 kW CW klystron amplifier, CESR-B type superconducting cavities and cryogenic system.

\*This manuscript has been authored by Brookhaven Science Associates, LLC under Contract No. DE-SC0012704 with the U.S. Department of Energy

<sup>†</sup> gwang@bnl.gov

LLRF controller was developed at NSLS-II and is based on modern FPGA technology. The field controller consists of six RF input channels, which are digitized by ADCs clocked at 4 MHz sampling rate. It is capable of generating set-point tables and finely controls of RF feedback parameters. With flexible and fast digital LLRF controller, the cavity phase and amplitude can be manipulated on a short timescale. Once triggered by outside timing event, the RF phase and amplitude data both before and after the event are captured by LLRF circular buffer and exported into EPICS system for offline analysis.

Figure 1 shows the LLRF block diagram. The RF set-point consists of I and Q (or phase and amplitude). RF cavity loop can operate in either feedforward (FF) or feedback (FB) modes. In the FF mode, the FF tables are loaded from outside and added with the normal feedback operating point to drive the klystron and subsequently cavity field. In the FB mode, cavity loop includes the inputs of RF setpoints, cavity pickup field and gain control parameters ( $K_p$ , proportional gain and  $K_i$ , integral gain). For the RF jump, it is in the feedback mode by switching RF setpoint between operating values and jump values. The gain parameters control the cavity field and the length of phase transition during RF jump.

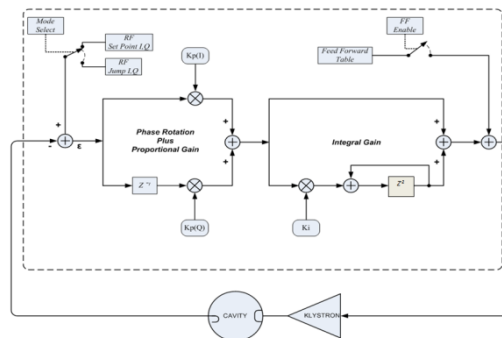


Figure 1: LLRF block diagram.

There is one button BPM installed next to RF cavity. Its raw data are processed to retrieve beam intensity and arrival time. The data are exported into circular buffer along with cavity phase and amplitude.

## MODEL OF LONGITUDINAL BEAM DYNAMICS WITH RF PINGER

Ideally, we would like to excite synchrotron oscillations instantaneously. However the speed of RF jump is limited by transmitter trips due to high reflected power or waveguide arcs.

Figure 2 shows the beam phase space evolution during RF phase jump at same phase jump amplitude, but differ-

ent transition period using linear ramp of RF phase. Blue trace corresponds to the long transition period (a few synchrotron periods), red trace shows  $\frac{1}{4}$  of synchrotron period and the black trace refers to a few ring turns-long transition of phase. The model was tested with various ramp profiles including the actual measured RF phase and amplitude transition and we chose the RF jump in the range of  $\frac{1}{4}$  of synchrotron period for our experiment.

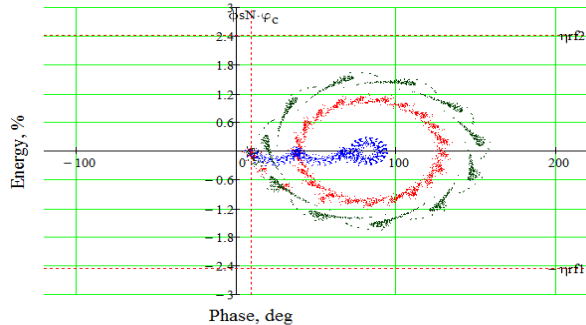


Figure 2: Model of longitudinal beam dynamics, beam evolution under slow (blue), medium (red) and fast (black) RF jump transition.

### RF PINGER IMPLEMENTATION

To accommodate the RF jump, the LLRF controller was modified by adding required controls and external on-demand timing trigger to control the jump event. Once the event is triggered, RF circular buffer is frozen to capture data both before and after the trigger event. It includes 8 channels' RF cavity signal and 2 channels' beam signals with 1.7 M waveform length at high rate data acquisition. To monitor the beam motion along SR due to RF pinger excitation the timing delay was aligned with BPMs sum signal so that RF pinger trigger is delayed by 100 turns relative to SR BPMs, and transverse pinger is delayed by 20 turns.

RF gain parameters  $K_p$  and  $K_i$  were also optimized so that the jump transition period was in the range of  $\frac{1}{4}$  of synchrotron period as required by the model above. It is observed that RF phase jump is coupled with RF amplitude.

SR RF cavity is over coupled at low beam current by design. The maximum RF phase jump amplitude is limited by high reflection power, which may cause RF transmitter trips. To reduce reflection power at low beam current, a 3- stub tuner has been added to raise the cavity  $Q_{ext}$  from 79k to 200k. This helps to increase the phase jump amplitude from 80 degree to 160 degree.

### RF PINGER STUDIES IN NSLS II

After we commissioned RF pinger at NSLS-II, we used this tool in several experiments. Below we discuss the data processing and obtained results on momentum aperture and rapid crossing half integer resonance.

#### Data Processing

Beam energy oscillation  $\delta$  from RF phase jump is measured with BPM located in dispersive region (from the optics model the dispersion is 0.42 m of  $\eta_1$  and -3 m of  $\eta_2$ ). When  $\delta$  is in the range of 2%, the beam position oscillates to the extent of 10 mm and the contributions from the second order dispersion cannot be ignored.

At so large beam offsets, 5<sup>th</sup> order correction needs to be applied to process the TBT data:

$$x_{mea} = p_{10} \left( \frac{\Delta}{\Sigma} \right)_x + p_{30} \left( \frac{\Delta}{\Sigma} \right)_x^3 + p_{50} \left( \frac{\Delta}{\Sigma} \right)_x^5$$

In addition the beam position depends on  $\delta$  as  $x = \eta_1 * \delta + \eta_2 * \delta^2$ . The energy oscillation written in terms of position is:

$$\delta = \frac{2x}{\left( \eta_1 + \sqrt{\eta_1^2 + 4\eta_2 x} \right)}$$

This solution is convenient for using in both linear and linear and 2<sup>nd</sup> order dispersion cases.

With the above 2-step data processing, the beam energy motion can be retrieved from TBT beam position data.

### Momentum Aperture Studies

Measurements of SR momentum aperture are important for modern light sources, since the beam lifetime is dominated by Touschek effect. Momentum aperture is limited by either physical aperture or dynamic aperture or RF momentum acceptance. It was studied in other facilities and measured in details at ALS [9] by statically moving beam off energy from RF frequency shift. At NSLS-II we measured the ring momentum aperture with RF pinger.

NSLS-II physical aperture is larger than the other two limitations. With RF cavities voltage in full operation value, its momentum aperture is designed as  $>2.6\%$ , ultimately limited by the dynamic aperture. In our study, we tested two cases, RF momentum aperture limitation with one RF cavity by closing or opening gaps of 3 damping wigglers and, separately, for two RF cavities without IDs.

**Experiment I: RF momentum aperture limitation.** In this test, our RF cavity C operated at 1.77 MV. NSLS-II energy loss per turn changes from 286 keV with damping wiggler gaps fully open to 412 keV with three DWs gaps closed. This provides the RF momentum aperture (same as RF bucket height) at 2.4% and 1.8% respectively. In both cases, the RF momentum aperture is smaller than dynamic or physical apertures.

We increased the RF phase jump amplitude gradually until the beam energy oscillation reaches momentum aperture limit and beam was lost. The measurement results are shown in Figure 3.

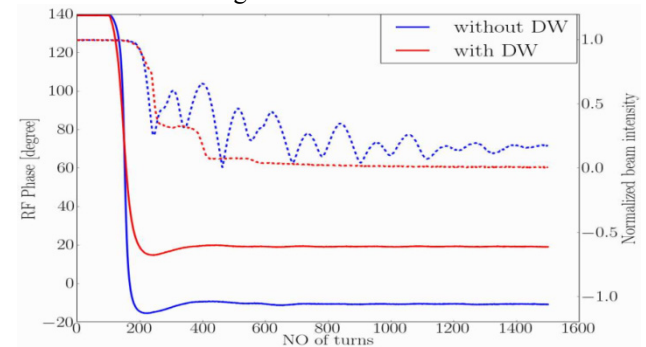


Figure 3: RF momentum aperture measurement without and with DW.

SR BPMs turn by turn sum signal are used to monitor the beam loss. SR BPMs tbt positions X are used to measure the actual beam energy oscillation. The BPMs sum signal showed that without DW, beam lost with

phase jump at 150 degree and the measured  $dE_{\max}$  is 2.4%.

With DWs, we lost beam with phase jump at 120 degree and the measured  $dE_{\max}$ , 1.8%.

**Experiment 2: Dynamic aperture limitation.** In this test, we run both RF cavities with the total voltage at 2.2 MV and DW fully open. The RF bucket height is 2.8%, larger than SR dynamic aperture. It required beam energy excitation larger than 2.6% to measure the dynamic aperture. At the same time the phase jump amplitude is limited to be 80 degree due to RF reflection power caused trip, which corresponds to only 1.2% in  $\delta$ . To reach the limit set by the dynamic aperture, the RF frequency was shifted statically to set the beam off-momentum in addition to the RF jump.

The results are shown in Fig. 4. The left plot shows one BPM TBT intensity and beam position oscillation. As predicted, the beam loss only happens in one side of the energy oscillations with synchrotron period. To find out where the dynamic aperture limit locates in the ring, we firstly zoom in a small region corresponding to beam loss and then selected this region of a few turns from all 180 BPMs for analysis.

The BPM sum signal exhibited level of noise in excess of slow loss rate due to the RF jump. Even with the normalized sum data BPM-to-BPM noise is still comparable with the beam loss in one turn and it is hard to judge where the beam is actually lost. To reduce the noise, the raw data was further processed by moving data average method. First, 180 BPMs different turns data was expanded into a long transport line in BPM sequence and turn sequence, as:  $I_{raw} = [I_i^{p1}, \dots, I_i^{pn}, I_{i+1}^{p1} \dots]$ , where  $pn$  is the BPM index number and  $i$  is the turn number. Then beam sum signal was processed via moving average as  $\bar{I}_i^{pj} = \text{mean}(I_i^{pj}, \dots, I_i^{pj+k})$ , where  $k$  is the slice number of averaged BPMs. The beam loss locations (Fig. 4) are pointed by sudden slope changes in the sum signal. The data points to the location of EPU ID in cell 23 of NSLS-II ring.

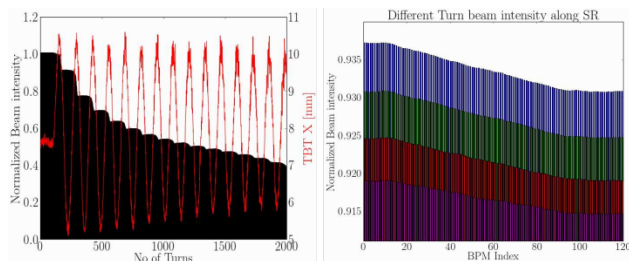


Figure 4: dynamic aperture limit location.

### Experiment on Crossing Half Integer Resonance

Modern light sources require large momentum aperture to keep good lifetime and large acceptance available for injection. Modern MBA lattices may exhibit large off-energy tune footprint with tune swing crossing major resonances. With the help of RF jump we developed an experiment where we show lossless or otherwise crossing

16½ vertical resonances via controlling the resonance stopband.

We modified the lattice working point to mimic machine tune footprint crossing half integer by creating high 2<sup>nd</sup> order chromaticity and excited beam energy oscillation using the RF phase jump. The sextupoles was optimized so that the y plane chromaticity is  $\xi_{y1} \sim 1$  and  $\xi_{y2} \sim 300$ . The y plane on-energy tune  $\nu_{y0}$  was moved to proximity to half integer and by pinging the RF phase the tune swung as:

$$\nu_y(i) = \nu_{y0} + \xi_{y1} * \delta(i) + \xi_{y2} * \delta(i)^2$$

where  $\delta(i)$  is energy oscillation at  $i^{\text{th}}$  turn, measured from BPM TBT position data. We controlled lattice stopband width by adjusting harmonic quadrupole strength. The measurement result as shown in figure 5 for two stopband half-widths of 0.015 and 0.03. The nominal tune was varied with respect to the resonance stopband and the TBT data was recorded. It shows that with small resonance stopband width, beam can cross half integer without loss and vice versa for the wider stopband.

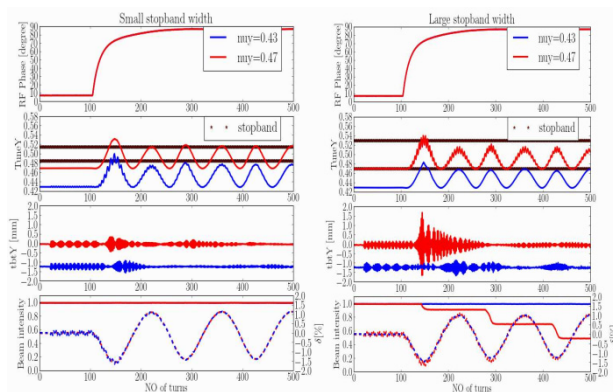


Figure 5: Beam crossing major resonance with stopband width control.

## SUMMARY AND OUTLOOK

High precision RF pinger system was commissioned and implemented at NSLS-II. This tool enables various beam dynamics studies that require transient excitation of synchrotron oscillations.

We plan more beam studies with RF pinger including harmonic excitation of coherent beam motion or measurements synchrotron motion as a function of beam current.

## ACKNOWLEDGMENT

I would like to acknowledge my colleagues, Feng Gao, Brian Holub, Carlos Marques, John Cupolo, Anton Derbenev, Juri Tagger, Weixing Cheng and Weiming Guo for their supports. Special thanks to Ferdinand Willeke for advice and discussions.

## REFERENCES

- [1] J. E. Griffin, "Synchrotron Phase Transition Crossing Using an RF Harmonic", FERMILAB-TM-1784.
- [2] K. Kubo and T. Okugi, "Dispersion Measurement in ATF DR", ATF Internal Report ATF-97-19 (1997).
- [3] Timur Shaftan, private communication.

- [4] T. Shaftan, “NSLS-II Accelerator Commissioning and Transition to Operations,” presented at the 7th Int. Particle Accelerator Conf. (IPAC’16), Busan, Korea, May 2016, paper WEPOY05.
- [5] G-M Wang, T. Shaftan, et.al, Rev. Sci. Instrum. 87, 033301 (2016).
- [6] F. Gao, et.al, “COMMISSIONING AND EARLY OPERATION EXPERIENCE OF THE NSLS-II STORAGE RING RF SYSTEM”, IPAC2015, WEPWI052.
- [7] J. Rose, et.al, NSLS-II RF SYSTEMS”, PAC2011, FROBS4.
- [8] B. Holub, et.al, “NSLS-II DIGITAL RF CONTROLLER LOGIC AND APPLICATIONS”, IPAC2015, MOPTY038.
- [9] C. Steier, Phys. Rev. E 65, 056506